Model-Free Simplified Predictive Current Control of PMSM Drive with Ultra-Local Model-Based EKF

Emrah Zerdali
Electrical and Electronics Engineering Department
Ege University
Izmir, Turkey
emrah.zerdali@ege.edu.tr

Patrick Wheeler
Electrical and Electronics Engineering Department
The University of Nottingham
Nottingham, NG7 2RD, U.K.
pat.wheeler@nottingham.ac.uk

***Abstract*—The importance of permanent magnet synchronous machines (PMSMs) is increasing day by day due to trends in the electrification of transportation and the use of wind farms. The predictive current control (PCC) strategy has been widely applied to the control of power converters and electrical machines over the past decade. However, parameter dependency and computational complexity are known disadvantages of the conventional PCC strategy. To deal with the weakness caused by parameter inconsistencies, model-free PCC strategy has been proposed. The simplified PCC strategies have also been applied to reduce computational complexity. In this paper, a model-free simplified PCC (MF-SPCC) strategy combined with the ultra-local model-based extended Kalman filter (EKF) has been proposed for a PMSM drive. The proposed electric drive system has been verified by simulation studies and finally robust control performance has been achieved under parameter mismatches.**

***Index Terms*—Model-free predictive current control, permanent magnet synchronous motor, extended Kalman filter, lumped parameter estimation**

I. Introduction

Compared to other machines, permanent magnet synchronous machines (PMSMs) provide some advantages such as higher power density, lower inertia, higher efficiency, and higher torque-to-weight ratio [1]. Their importance has increased due to the trends in the electrification of transportation [2], [3] and the use of wind farms [4], [5]. However, their highly nonlinear structures with time-varying parameters complicate their high-performance control; therefore, advanced control techniques are needed. Field-oriented control (FOC) and direct torque control (DTC) have been used for their high-performance control for a long time [6]. Although these techniques are still in use extensively, the latest model predictive control (MPC) techniques, predictive current control (PCC) and predictive torque control (PTC), provide many advantages over mature control techniques, such as easy concept, fast response, the capability of handling nonlinearities, modulator-free structure, easy inclusion of additional control objectives [7]. A comparison of all these high-performance control techniques has been made for induction motor control in [8]. In a comparison between the PCC and PTC, it is highlighted that the PCC has lower computational complexity and current harmonics although they have similar performances [7].

Despite all advantages of the PCC strategy, it has some drawbacks reported in the literature: current harmonics, variable switching frequency, computational complexity, and parameter dependency [9]. To deal with these problems, effective solutions have been proposed. Current harmonics can be suppressed by using higher-order converter topologies, sacrificing computational complexity and cost [10], [11]. However, the two-level voltage source inverter (2L-VSI) topology still remains popular in electric drive systems. Also, unlike the traditional PCC strategy, applying multiple vectors during one sampling period can suppress current harmonics [12]. Another solution to greatly overcome both current harmonics and variable switching frequency is to use modulated PCC strategies [10], [13]. It is clear that these solutions damage the basic structure of traditional PCC. To reduce the computational complexity, simplified PCC strategies have been proposed that reduce the number of candidate switching states [10], [11] or the number of predicted quantities [14]. There are some studies using nonlinear observers such as recursive least squares (RLS) filter [15] and extended Kalman filter (EKF) [16] to overcome the problem of parameter changes. However, it is emphasized that estimating a few or all parameters is not a cost-effective solution [17]. However, it can be a reasonable option where parameter changes are required. The problem of parameter dependency can be significantly eliminated by using the incremental model [18] or model-free PCC strategies [11], [13], [19], [20]. The main disadvantage of incremental model-based PCC is the necessity of measuring current twice in one sampling period [20]. Model-free PCC strategies require a disturbance observer as they use the ultra-local model [18]–[20]. In the literature, there are different studies combining disturbance observers based on extended state observer [18], [20] and nonlinear observer [19] with model-free PCC strategies.

In this paper, a model-free simplified PCC strategy combined with EKF-based on the ultra-local model of PMSM has been proposed for PMSM drives. The EKF observer used is capable of estimating known and unknown interference terms in the ultra-local model of PMSM. The proposed PMSM drive is robust to parameter changes and its computational load has also been reduced by adopting simplified PCC strategy. Finally, it is validated through extensive simulation studies.

The rest of this paper is organized as follows: Section II gives the detail of the ultra-local model for PMSM. Section

978-1-6654-3512-3/21/$31.00 © 2021 IEEE

III presents the design steps of the EKF observer based on the ultra-local model. Section IV introduces the MF-SPCC combined with EKF observer for PMSM drives. Section V validates the proposed PMSM drive through simulation studies, followed by the conclusion in Section VI.

II. Ultra-Local Model of PMSM

The mathematical model of surface-mounted PMSM (SPMSM) consists of two sub-models: the electrical model and the mechanical model. The set of equations for this model is given in (1).

$$\frac{di_d}{dt} = -\frac{R_s}{L_s} i_d + \omega_r i_q + \frac{u_d}{L_s} \tag{1a}$$

$$\frac{di_q}{dt} = -\frac{R_s}{L_s} i_q - \omega_r i_d + \frac{u_q}{L_s} - \frac{1}{L_s}\omega_r \psi_{\rm pm} \tag{1b}$$

$$\frac{d\omega_m}{dt} = \frac{3}{2}\frac{p_p}{J_t}\psi_{\rm pm} i_q - \frac{B_t}{J_t}\omega_m - \frac{\tau_l}{J_t} \tag{1c}$$

where i_d and i_q are the $dq-$axis components of stator currents, u_d and u_q are the $dq-$axis components of stator voltages, ω_m is the mechanical angular speed, $\omega_r = p_p\omega_m$ is the electrical angular speed, p_p is the number of pole-pairs, $\psi_{\rm pm}$ is the rotor flux linkage of permanent magnets, τ_l is the load torque, R_s and L_s are the stator resistance and inductance, respectively, B_t and J_t are the inertia and viscous friction, respectively.

Rearranging the model in (1), the voltage equations can be found as

$$u_d = R_s i_d + L_s\frac{di_d}{dt} - L_s\omega_r i_q \tag{2a}$$

$$u_q = R_s i_q + L_s\frac{di_q}{dt} + L_s\omega_r i_d + \omega_r\psi_{\rm pm} \tag{2b}$$

To realistically define the PMSM model, the voltage equations can be expanded by parameter mismatches and unknown interference terms as

$$u_d = (R_s + \Delta R_s) i_d + (L_s + \Delta L_s)\frac{di_d}{dt} - (L_s + \Delta L_s)\omega_r i_q + \lambda_d \tag{3a}$$

$$u_q = (R_s + \Delta R_s) i_q + (L_s + \Delta L_s)\frac{di_q}{dt} + (L_s + \Delta L_s)\omega_r i_d + \omega_r(\psi_{\rm pm} + \Delta\psi_{\rm pm}) + \lambda_q \tag{3b}$$

where ΔR_s, ΔL_s, and $\Delta\psi_{\rm pm}$ are parameter mismatches, λ_d and λ_q are unknown terms for the electrical side of the PMSM model. Rearranging (3) gives

$$\frac{di_d}{dt} = \frac{u_d}{L_s} + \left(- \frac{\Delta L_s}{L_s}\frac{di_d}{dt} - \frac{(R_s + \Delta R_s)}{L_s} i_d + \frac{(L_s + \Delta L_s)}{L_s}\omega_r i_q - \frac{\lambda_d}{L_s}\right) \tag{4a}$$

$$\frac{di_q}{dt} = \frac{u_q}{L_s} + \left(- \frac{\Delta L_s}{L_s}\frac{di_q}{dt} - \frac{(R_s + \Delta R_s)}{L_s} i_q - \frac{(L_s + \Delta L_s)}{L_s}\omega_r i_d - \omega_r\frac{(\psi_{\rm pm} + \Delta\psi_{\rm pm})}{L_s} - \frac{\lambda_q}{L_s}\right) \tag{4b}$$

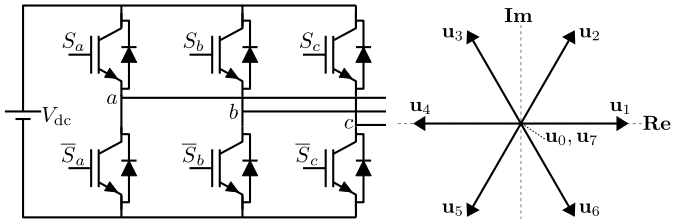

(a) (b)

Fig. 1. 2L-VSI (a) Circuit topology (b) Possible voltage vectors

Using the model in (4), the ultra-local PMSM model based on the system input and output data can be constructed for the electrical side as follows:

$$\frac{di_d}{dt} = \xi u_d + \Lambda_d \tag{5a}$$

$$\frac{di_q}{dt} = \xi u_q + \Lambda_q \tag{5b}$$

where $\xi = 1/L_s$ is the gain of the inputs, Λ_d and Λ_q are the sums of known and unknown terms for the electrical side of the PMSM model and are given as follows:

$$\Lambda_d = -\frac{\Delta L_s}{L_s}\frac{di_d}{dt} - \frac{(R_s + \Delta R_s)}{L_s} i_d + \frac{(L_s + \Delta L_s)}{L_s}\omega_r i_q - \frac{\lambda_d}{L_s} \tag{6a}$$

$$\Lambda_q = -\frac{\Delta L_s}{L_s}\frac{di_q}{dt} - \frac{(R_s + \Delta R_s)}{L_s} i_q - \frac{(L_s + \Delta L_s)}{L_s}\omega_r i_d - \frac{(\psi_{\rm pm} + \Delta\psi_{\rm pm})}{L_s}\omega_r - \frac{\lambda_q}{L_s} \tag{6b}$$

If a 2L-VSI is applied to the PMSM, the output voltage of the inverter in the stator stationary reference frame ($\alpha\beta-$) can be calculated as

$$\mathbf{u}_{s,\alpha\beta} = \frac{2}{3} V_{\rm dc}(S_a + aS_b + a^2 S_c) \tag{7}$$

where $V_{\rm dc}$ is the dc-link voltage, $S_x \in \{S_a, S_b, S_c\}$ is the switching state of the upper switch on each leg, a is the phase shift of 120 electrical degrees. It is also possible to define the $\mathbf{u}_{s,\alpha\beta}$ in the rotating reference frame ($dq-$) as follows:

$$\mathbf{u}_{s,dq} = \mathbf{u}_{s,\alpha\beta} \cdot e^{-j\theta_r} \tag{8}$$

where θ_r is the electrical rotor position of the PMSM. The circuit topology of 2L-VSI and possible voltage vectors are given in Fig. 1.

III. EKF Observer

To estimate the Λ_d and Λ_q, the ultra-local PMSM model in (5) has been extended by these interference terms and a nonlinear PMSM model in (9) has been derived. Next, an EKF observer has been designed based on the extended ultra-local model of PMSM. The reason for using the EKF observer is that the model in (9) is nonlinear and EKF has

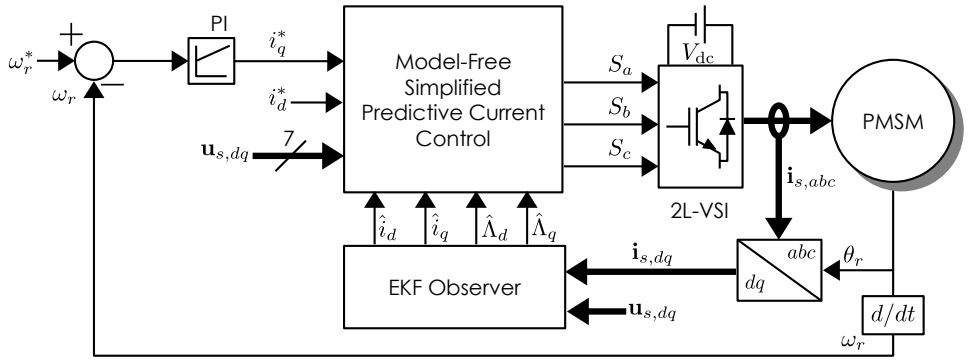

Fig. 2. Block diagram of the SPMSM drive based on the MF-SPCC combined with EKF observer

lower computational complexity than other nonlinear Kalman filtering methods [21].

$$\underbrace{\begin{bmatrix}\dot{i}_d\\ \dot{i}_q\\ \dot{\Lambda}_d\\ \dot{\Lambda}_q\end{bmatrix}}_{\dot{\mathbf{x}}_t} = \underbrace{\begin{bmatrix}\xi u_d + \Lambda_d\\ \xi u_q + \Lambda_q\\ 0\\ 0\end{bmatrix}}_{\mathbf{f}(\mathbf{x}_t,\mathbf{u}_t)} \tag{9}$$

The nonlinear model in (9) has to be discretized in order to use in the EKF and first-order Euler approximation

$$\dot{\mathbf{x}}_t \approx \frac{\mathbf{x}_{k+1} - \mathbf{x}_k}{T} \tag{10}$$

has been used in this paper. The resulting observer model in discrete form is

$$\mathbf{x}_{k+1} = \mathbf{I}_{4\times 4} \cdot \mathbf{x}_k + T \cdot \mathbf{f}(\mathbf{x}_t, \mathbf{u}_t) \tag{11}$$

where $\mathbf{I}$ is the identity matrix and T is the sampling time. The remaining steps for the EKF observer are as follows:

1- Initialization step:

$$\hat{\mathbf{x}}_0^- = E[\mathbf{x}_0] \tag{12}$$

$$\mathbf{P}_0 = E[(\mathbf{x}_0 - E[\mathbf{x}_0])(\mathbf{x}_0 - E[\mathbf{x}_0])^T] \tag{13}$$

2- Linearization step:

$$\mathbf{F}_{k+1|k} = \left.\frac{\partial \mathbf{f}(\mathbf{x}, \mathbf{u}_k)}{\partial \mathbf{x}}\right|_{\mathbf{x}=\mathbf{x}_k} \tag{14}$$

3- Time update:

$$\hat{\mathbf{x}}_k^- = \mathbf{f}(\hat{\mathbf{x}}_{k-1}, \mathbf{u}_k) \tag{15}$$

$$\mathbf{P}_k^- = \mathbf{F}_{k|k-1}\mathbf{P}_{k-1}\mathbf{F}_{k|k-1}^T + \mathbf{Q}_{k-1} \tag{16}$$

4- Measurement update:

$$\mathbf{K}_k = \mathbf{P}_k^-\mathbf{H}^T\left[\mathbf{H}\mathbf{P}_k^-\mathbf{H}^T + \mathbf{R}_k\right]^{-1} \tag{17}$$

$$\hat{\mathbf{x}}_k = \hat{\mathbf{x}}_k^- + \mathbf{K}_k\mathbf{v}_k \tag{18}$$

$$\mathbf{P}_k = (\mathbf{I} - \mathbf{K}_k\mathbf{H})\mathbf{P}_k^- \tag{19}$$

where $\mathbf{F}_{k|k-1}$ is the transition matrix; $\mathbf{P}_k^-$ and $\mathbf{P}_k$ are the priori and the posteriori covariance matrices, respectively; $\mathbf{K}_k$ is the Kalman gain; $\mathbf{Q}_k$ and $\mathbf{R}_k$ are the covariance matrices of the system noise and the output noise, respectively.

TABLE I
THE SPECIFICATION OF PMSM

Parameter	Value	Parameter	Value
n_m	2300 [r/min]	τ_l	10 [N.m]
p_p	4	$\psi_{\rm pm}$	0.171 [V.s]
R_s	0.4578 [Ω]	L_s	3.34 [mH]
J_t	0.001469 [kg.m^2]	B_t	0.0003035 [N.m.s]

TABLE II
SIMULATION PARAMETERS

Parameter	Symbol	Value
Sampling time	T	50μs
Proportional gain	K_p	5
Integral gain	K_i	50
DC-link voltage	$V_{\rm dc}$	300 V
System noise covariance matrix	$\mathbf{Q}$	diag $\{1, 1, 0.1, 0.1\}$
Measurement noise covariance matrix	$\mathbf{R}$	diag $\{1, 1\}$
Initial posteriori covariance matrix	$\mathbf{P}_0$	diag $\{1, 1, 1, 1\}$

IV. MF-SPCC OF PMSM WITH EKF OBSERVER

To perform the MF-SPCC strategy, the direct and quadrature-axis voltages can be obtained after the discretization and rearrangement of the ultra-local model in (5) as follows:

$$u_{d,k+1} = \frac{(i_{d,k+1} - i_{d,k})}{T\xi} - \frac{\hat{\Lambda}_{d,k+1}}{\xi} \tag{20a}$$

$$u_{q,k+1} = \frac{(i_{q,k+1} - i_{q,k})}{T\xi} - \frac{\hat{\Lambda}_{q,k+1}}{\xi} \tag{20b}$$

where $\hat{\Lambda}_d$ and $\hat{\Lambda}_q$ are the values of known and unknown interference terms estimated by the EKF.

Substituting reference currents (i_d^* and i_q^*) in (20), the reference voltages (u_d^* and u_q^*) can be obtained as

$$u_d^* = \frac{(i_d^* - i_{d,k})}{T\xi} - \frac{\hat{\Lambda}_{d,k+1}}{\xi} \tag{21a}$$

$$u_q^* = \frac{(i_q^* - i_{q,k})}{T\xi} - \frac{\hat{\Lambda}_{q,k+1}}{\xi} \tag{21b}$$

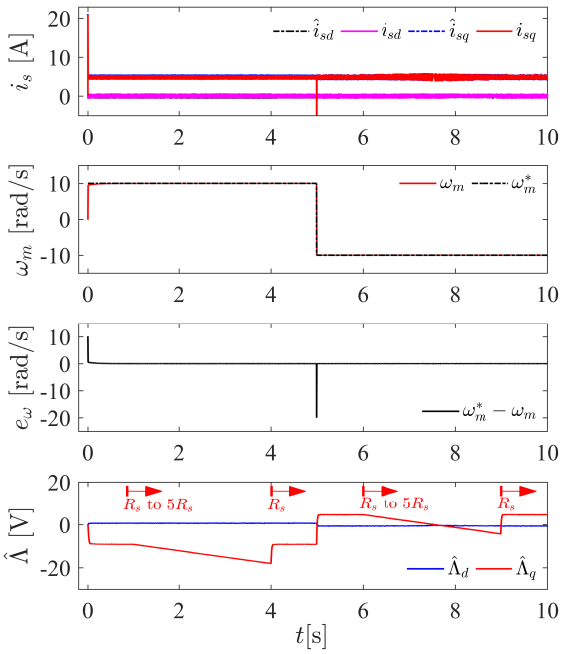

Fig. 3. Control performance under R_s changes

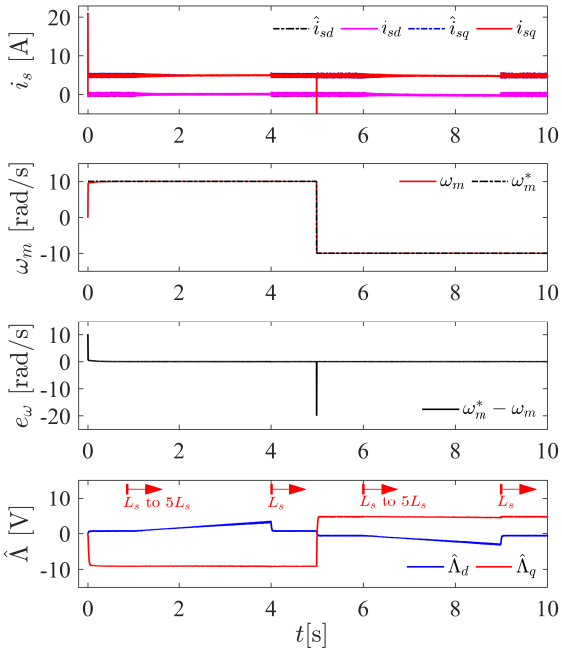

Fig. 4. Control performance under L_s changes

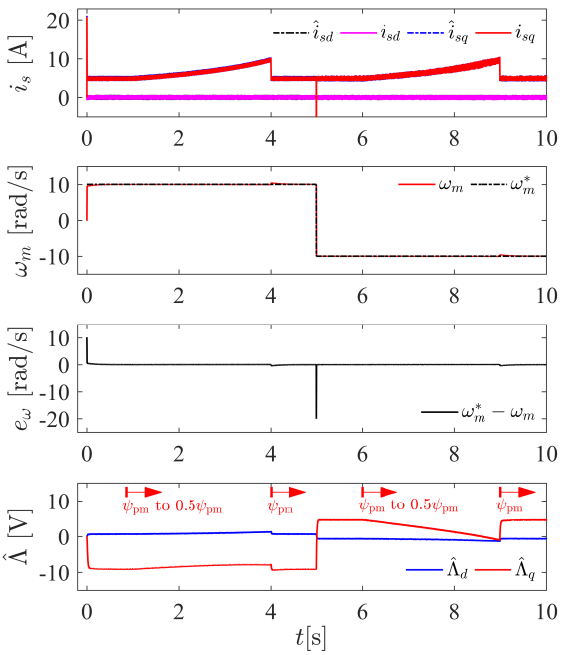

Fig. 5. Control performance under $\psi_{\rm pm}$ changes

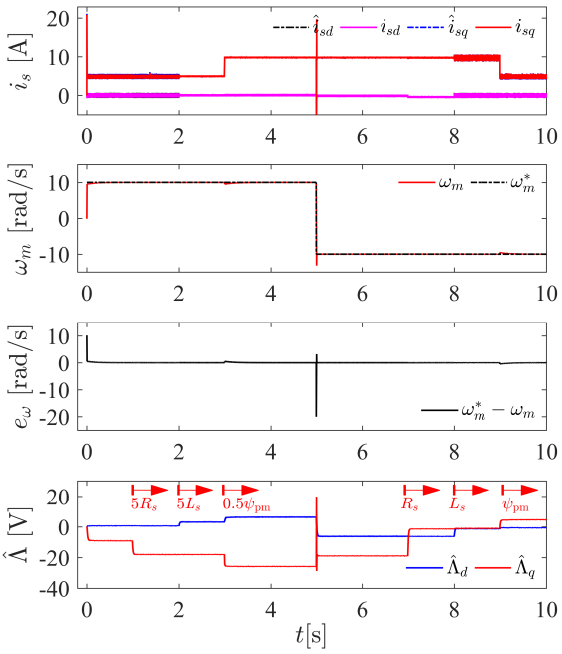

Fig. 6. Control performance under combined changes of R_s, L_s, and $\psi_{\rm pm}$

where $i_d^* = 0$ for SPMSM.

The optimal switching state for next time instant can eventually be selected with the following cost function:

$$g_j = \min_{j\in\{0,1,\ldots,7\}} \left\{(v_d^* - v_{d,j})^2 + (v_q^* - v_{q,j})^2\right\} \qquad (22)$$

V. Results

The block diagram of the SPMSM drive based on the MF-SPCC combined with the EKF is shown in Fig. 2 and a PMSM with the specifications in Table I is used in simulation studies. This SPMSM drive has been implemented in Matlab/Simulink. The speed controller is of PI-type. All values and parameters used in simulation studies are given in Table II.

In simulation studies, different operating conditions have been considered in order to demonstrate the effectiveness of the proposed SPMSM drive. To show its robustness against the parameter changes, the control performance has also been

examined under changes in R_s, L_s, and $\psi_{\rm pm}$.

In all results shown in Figs. 3–6, if χ is a dummy variable, $\hat{\chi}$ and χ^* indicate the estimated and reference quantities, respectively. In all tests, the speed is reversed from $+10$ rad/s to -10 rad/s at $t = 5$ s to show the speed-dependent interference terms. In Figs. 3 and 4, R_s and L_s are increased from their rated values to 5 times their rated values for time intervals of $1 \leq t \leq 4$ s and $7 \leq t \leq 9$ s. Also, step-type changes of both R_s and L_s from 5 times their rated values to their rated values have been performed at $t = 4$ s and $t = 9$ s. In Figs. 5, the $\psi_{\rm pm}$ is halved from its rated value for time intervals of $1 \leq t \leq 4$ s and $7 \leq t \leq 9$ s. Moreover, it is stepped up to its rated value at $t = 4$ s and $t = 9$ s. In the last test in Fig. 6, the proposed PMSM drive is tested with combined changes in parameters. To this end, R_s and L_s are stepped up to 5 times their nominal values at $t = 1$ s and $t = 2$ s, respectively. Next, $\psi_{\rm pm}$ is stepped down to half of its nominal value at $t = 3$ s. Finally, values of R_s, L_s, and $\psi_{\rm pm}$ are returned to their nominal values at $t = 7$ s, $t = 8$ s, and $t = 9$ s, respectively.

Considering the resulting control performances, it is shown that the proposed PMSM drive based on MF-SPCC with EKF can compensate for the adverse effects of parameter changes. The EKF has the ability to estimate the interference terms in the ultra-local model even under the ramp and step-type changes in parameters. The interference terms are not only related to parameter changes but also speed-dependent. As shown in all results, the $\hat{\Lambda}_d$ and $\hat{\Lambda}_q$ have different values at different speeds. In a realistic case, all these parameter and speed changes may occur at the same time as tested in Fig. 6. Even under these troubled operating conditions, the proposed electric drive system can still follow the reference variations with high performance.

VI. Conclusion

In this paper, a PMSM drive based on the MF-SPCC combined with the EKF has been proposed and tested in simulation studies under challenging operating conditions. Due to the use of ultra-local PMSM model that does not include parameters apart from L_s and the estimation of known and unknown interference terms with the EKF observer, it overcomes the problem of parameter dependency in the conventional PCC strategy. The simulation results demonstrate that it has the ability to operate with high performance under parameter mismatches at different speeds. It still has current harmonics and variable switching frequency caused by the limited number of switching states in power converters and the PCC strategy. Future studies will focus on addressing these issues.

References

[1] T. Turker, U. Buyukkeles, and A. F. Bakan, "A Robust Predictive Current Controller for PMSM Drives," *IEEE Trans. Ind. Electron.*, vol. 63, no. 6, pp. 3906–3914, 2016.

[2] S.-C. Carpiuc and C. Lazar, "Fast real-time constrained predictive current control in permanent magnet synchronous machine-based automotive traction drives," *IEEE Trans. Transp. Electrif.*, vol. 1, no. 4, pp. 326–335, 2015.

[3] P. Wheeler, T. S. Sirimanna, S. Bozhko, and K. S. Haran, "Electric/hybrid-electric aircraft propulsion systems," *Proceedings of the IEEE*, vol. 109, no. 6, pp. 1115–1127, 2021.

[4] V. Yaramasu and B. Wu, "Predictive control of a three-level boost converter and an npc inverter for high-power pmsg-based medium voltage wind energy conversion systems," *IEEE Trans. Power Electron.*, vol. 29, no. 10, pp. 5308–5322, 2014.

[5] S. Li and J. Li, "Output predictor-based active disturbance rejection control for a wind energy conversion system with pmsg," *IEEE Access*, vol. 5, pp. 5205–5214, 2017.

[6] F. Korkmaz, I. Topaloglu, M. F. Cakir, and R. Gurbuz, "Comparative performance evaluation of FOC and DTC controlled PMSM drives," in *4th International Conference on Power Engineering, Energy and Electrical Drives*, 2013, pp. 705–708.

[7] F. Wang, S. Li, X. Mei, W. Xie, J. Rodríguez, and R. M. Kennel, "Model-based predictive direct control strategies for electrical drives: An experimental evaluation of PTC and PCC methods," *IEEE Trans. Ind. Informatics*, vol. 11, no. 3, pp. 671–681, 2015.

[8] F. Wang, Z. Zhang, X. Mei, J. Rodríguez, and R. Kennel, "Advanced Control Strategies of Induction Machine: Field Oriented Control, Direct Torque Control and Model Predictive Control," *Energies*, vol. 11, no. 1, p. 120, 2018.

[9] M. F. Elmorshedy, W. Xu, F. F. El-Sousy, M. R. Islam, and A. A. Ahmed, "Recent Achievements in Model Predictive Control Techniques for Industrial Motor: A Comprehensive State-of-the-Art," *IEEE Access*, vol. 9, pp. 58 170–58 191, 2021.

[10] Q. Wang, H. Yu, C. Li, X. Lang, S. S. Yeoh, T. Yang, M. Rivera, S. Bozhko, and P. Wheeler, "A Low-Complexity Optimal Switching Time-Modulated Model-Predictive Control for PMSM with Three-Level NPC Converter," *IEEE Trans. Transp. Electrif.*, vol. 6, no. 3, pp. 1188–1198, 2020.

[11] F. Yu, C. Zhou, X. Liu, and C. Zhu, "Model-Free Predictive Current Control for Three-Level Inverter-Fed IPMSM with an Improved Current Difference Updating Technique," *IEEE Trans. Energy Convers.*, vol. 8969, no. c, pp. 1–1, 2021.

[12] C. Xiong, H. Xu, T. Guan, and P. Zhou, "A Constant Switching Frequency Multiple-Vector-Based Model Predictive Current Control of Five-Phase PMSM with Nonsinusoidal Back EMF," *IEEE Trans. Ind. Electron.*, vol. 67, no. 3, pp. 1695–1707, 2020.

[13] Y. Wang, H. Li, R. Liu, L. Yang, and X. Wang, "Modulated model-free predictive control with minimum switching losses for PMSM drive system," *IEEE Access*, vol. 8, pp. 20 942–20 953, 2020.

[14] C. Xia, T. Liu, T. Shi, and Z. Song, "A simplified finite-control-set model-predictive control for power converters," *IEEE Trans. Ind. Informatics*, vol. 10, no. 2, pp. 991–1002, 2014.

[15] A. Brosch, S. Hanke, O. Wallscheid, and J. Bocker, "Data-Driven Recursive Least Squares Estimation for Model Predictive Current Control of Permanent Magnet Synchronous Motors," *IEEE Trans. Power Electron.*, vol. 36, no. 2, pp. 2179–2190, 2020.

[16] R. Yildiz, M. Barut, and R. Demir, "Extended kalman filter based estimations for improving speed-sensored control performance of induction motors," *IET Electric Power Applications*, vol. 14, no. 12, pp. 2471–2479, 2020.

[17] F. Niu, X. Wang, S. Huang, X. Huang, L. Wu, K. Li, and Y. Fang, "Current Prediction Error Reduction Method of Predictive Current Control for Permanent Magnet Synchronous Motors," *IEEE Access*, vol. 8, pp. 124 288–124 296, 2020.

[18] M. Yang, X. Lang, J. Long, and D. Xu, "Flux immunity robust predictive current control with incremental model and extended state observer for PMSM drive," *IEEE Trans. Power Electron.*, vol. 32, no. 12, pp. 9267–9279, 2017.

[19] L. Xu, G. Chen, and Q. Li, "Ultra-Local Model-Free Predictive Current Control Based on Nonlinear Disturbance Compensation for Permanent Magnet Synchronous Motor," *IEEE Access*, vol. 8, pp. 127 690–127 699, 2020.

[20] Y. Zhang, J. Jin, and L. Huang, "Model-Free Predictive Current Control of PMSM Drives Based on Extended State Observer Using Ultralocal Model," *IEEE Trans. Ind. Electron.*, vol. 68, no. 2, pp. 993–1003, 2021.

[21] R. Yildiz, M. Barut, and E. Zerdali, "A Comprehensive Comparison of Extended and Unscented Kalman Filters for Speed-Sensorless Control Applications of Induction Motors," *IEEE Trans. Ind. Informatics*, vol. 16, no. 10, pp. 6423–6432, Oct. 2020.